



Crystal growth and characterization of 2-amino-6-methylpyridinium *p*-chlorobenzoate dihydrate single crystal: a novel third-order nonlinear optical material for optoelectronic applications

R. Kaliammal¹, G. Parvathy¹, G. Ravi¹, V. Mohan Kumar², M. Krishna Kumar³, and S. Sudhahar^{1,*}

¹Department of Physics, Alagappa University, Karaikudi 630003, India

²Nehru Institute of Technology, Coimbatore 641105, India

³Department of Physics, Kalasalingam Academy of Research and Education, Krishnankoil 626126, India

Received: 9 October 2021

Accepted: 22 December 2021

Published online:
30 January 2022

© The Author(s), under exclusive licence to Springer Science+Business Media, LLC, part of Springer Nature 2021

ABSTRACT

The organic single crystal of 2-amino-6-methylpyridinium *p*-chlorobenzoate dihydrate (2A6MP) single crystal was successfully grown by the slow evaporation method. The structural parameters of grown 2A6MP single crystal were confirmed by the single crystal X-ray diffraction technique. It revealed that 2A6MP crystal belongs to the centrosymmetric crystal structure with the space group of $P12_1/c1$. The crystallinity nature was confirmed by the powder XRD analysis. FT-IR spectroscopy was used to find out the presence of functional groups in the 2A6MP crystal. UV-Vis spectrometer analysis showed that 2A6MP crystal has a lower cut-off wavelength at 349 nm in the UV region and the 66% transmittance in the visible region ensured that the grown crystal is well suitable for nonlinear optical applications. From the photoluminescence spectrum, the emission peaks are at 378 nm in the violet region and 428, 478 nm in the blue region revealed the 2A6MP crystal is useful for violet and blue emitting diodes. The 2A6MP crystal was thermally stable upto the temperature rate of 106.8 °C was confirmed by the thermogravimetric/differential scanning calorimetric analysis. The mechanical properties of 2A6MP crystal were investigated using a Vickers microhardness tester, and the results revealed that the title compound has relates to the soft material category which is useful for optoelectronic applications. From the *Z*-scan technique, the third-order nonlinear properties such as nonlinear refractive index, nonlinear absorption co-efficient, and third-order susceptibility of the grown 2A6MP crystal was found to be $-4.25 \times 10^{-09} \text{ m}^2/\text{W}$ and $3.16 \times 10^{-04} \text{ m/W}$ and $4.95 \times 10^{-06} \text{ esu}$. All of these investigations were carried out for the first time, with the goal of determining the useful and safe range of thermal, optical, and mechanical properties

Address correspondence to E-mail: sudhahars@alagappauniversity.ac.in

in order to improve their usefulness for device production. Density functional theory (DFT) was carried out using Gaussian 09 program with the basis set of B3LYP/6-311++G(*d*, *P*), to find out the molecular geometry, frontier molecular orbital energies, molecular electrostatic potential, Mulliken, and natural bond orbital analysis of the grown 2A6MP crystal theoretically and it ensures the intermolecular charge transfer mechanism of 2A6MP crystal that induced the nonlinearity.

1 Introduction

In recent decades, organic materials usage in nonlinear optical applications is increased by compared with inorganic counterparts. This was due to their advantages of the π -conjugated molecular system, large resistance damage, and high electro-optics coefficient, structural flexibility, and excellent nonlinear optical efficiency [1–4]. Hence now it has much attention in the field of optical oriented power limiting, 3-dimensional memory devices, and optical switching applications, laser moderation, optical computing, optical communications, and sensing [5–8]. Hence, the researchers are focused to develop the organic single crystal growth for technological applications [9]. The organic molecules possess hydrogen donor and acceptor groups as conjugated structures. Thus groups are lead to the various approach of hydrogen bonding through acid and base groups in organic structures that gives the nonlinearity due to their molecule charges become asymmetry [10]. Hence the material's nonlinearity was considerably improved by the strong donor to acceptor electronic transition in delocalized electrons also the π - π stacking, hydrogen bonding, and intramolecular charge transfer [11, 12] are the most important factors in increasing a molecule's nonlinear activity [13, 14]. Pyridine derivatives are an example of an organic substance that easily forms stable complexes with a suitable donor. This impact has also been reported previously using a variety of organic compounds, such as carboxylic acid and other acids derivatives. Among the organic materials, the presence of nitrogen in the pyridine ring is also known to enhance the creation of salts during interaction with certain organic acids which could exhibit efficient second and third-order nonlinearity [15, 16]. Pyridine compounds are also important in biology because they have a variety of biological effects,

including anticancer, antibiotic, psychotropic, anti-inflammatory, and antihistaminic capabilities [17]. Furthermore, pyridine compounds show promise in organic semiconductors, optoelectronics, photophysical, catalysis, in addition to electrochemical applications [18–20]. Benzoic acid derivatives are an important part of the vitamin B complex. Benzoic acid, like vitamin B-complex, is found widely in plant and animal tissues and is employed in miticides, Cholecystographic examinations, contrast media in urology, and pharmaceuticals manufacture [21]. *p*-, *m*-, and *o*-chlorobenzoic acid's IR and Raman spectra were previously examined in solid form and in various solutions. The vibrational assignments of chlorobenzoic acids have been postulated based on group frequency, band shape, intensity, and some internal consistency. Chlorobenzoic acids exist as hydrogen bond dimers in solids and monomeric acids in organic solvents such as chloroform, diethyl ether, ethanol, according to studies of carboxylic acid and carboxylate vibrations whereas in sodium hydroxide solutions as carboxylate ions. In the case of halogens, the inductive effect dominates over the resonance effect. As a result of the Cl on the para position, *p*-chlorobenzoic acid should be more acidic than benzoic acid due to the *I* effect [22]. The ICT transfer of pyridine to benzoic acid derives single crystals such as 2-amino 4-picolinium 4-aminobenzoate [23], 2-amino-6-methylpyridinium 3,4-dimethoxybenzoate [24], 2-aminopyridinium 2-chloro 4-nitro benzoate [25], and 2-amino-6-methylpyridinium 4-nitrobenzoate [26] exhibited the second and third-order nonlinearity. Hence we have selected the parent compound of 2-amino-methylpyridine, *p*-chlorobenzoic acid in this series to grow the 2-amino-6-methylpyridinium *p*-chlorobenzoate dihydrate organic single crystal. The grown 2A6MP crystal physicochemical properties such as structural, functional, optical, thermal, mechanical, and third-order nonlinear responses are analyzed. 2A6MP

crystal is a good candidate for practical NLO device applications particularly for optoelectronic devices. DFT analysis on the grown single crystal supports ICT interactions between the hydrogen donor and acceptor molecular groups which induce the nonlinearity and the detailed discussions are presented in this article.

2 Experimental section

2.1 Material synthesis and crystal growth

As shown in the synthesis scheme of Fig. 1a, the organic 2-amino-6-methylpyridinium *p*-chlorobenzoate dihydrate single crystal was generated from the parent compound of 2-amino-6-methylpyridine (2A6M) and *p*-chlorobenzoic acid (P) in an equimolar ratio of 1:1. Initially, 2.4 g of *p*-chlorobenzoic acid was dissolved in 50 ml of ethanol. Subsequently, 2.8 g of 2-amino-6-methylpyridine was added into the *p*-chlorobenzoic acid solution. Then the mixed solution (2A6MP) was stirred well to get the homogeneous mixture. After that the attained 2A6MP solution was

allowed to the solution crystal growth technique by the slow evaporation method. The recrystallization process was repeated three times to get the pure crystal. The slow evaporation yields the 2A6MP crystal with the size of about $20 \times 10 \times 10 \text{ mm}^3$ within 3–4 weeks as shown in Fig. 1b.

2.2 Solubility study

The solubility study was carried out for the prepared compound of 2A6MP in ethanol at different temperatures. The solvent selection and the suitable temperature are the most important pre-requisite for obtaining bulk size single crystals. First the less amount of 2A6MP sample “solute” was added slowly into the 100 ml of ethanol solvent at 30 °C. The saturation of the solute represents the maximum solute at the taken 100 ml solvent was found and noted. The same procedure was applied to the remaining planned temperatures of 35 °C, 40 °C, 45 °C, and 50 °C. The entire solubility test results are plotted as the graph and shown in Fig. 2. The results reveal the amount of solute was increased with respect to the

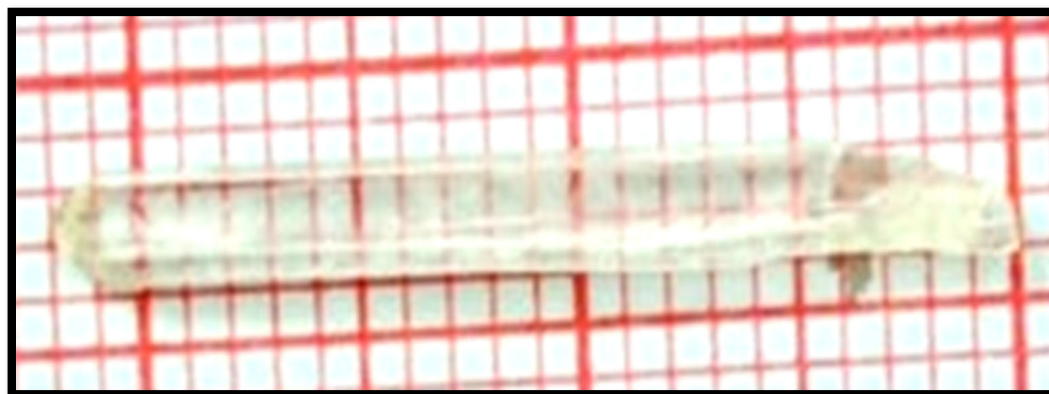
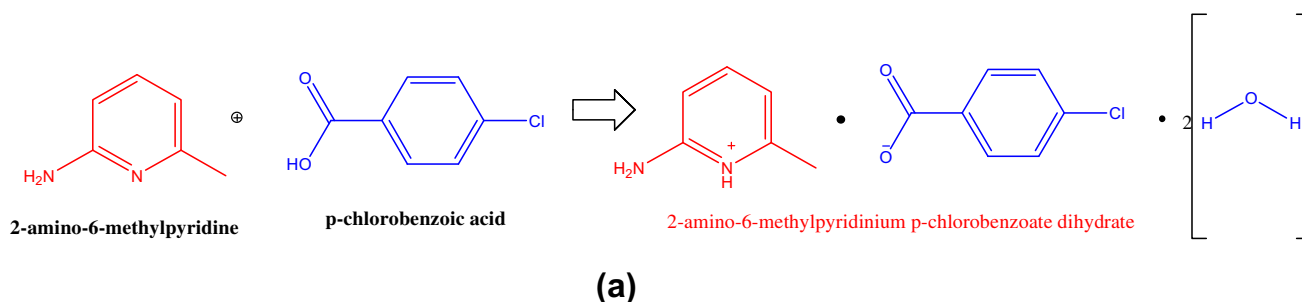


Fig. 1 a A synthesis scheme and b Photograph of as-grown 2A6MP single crystal

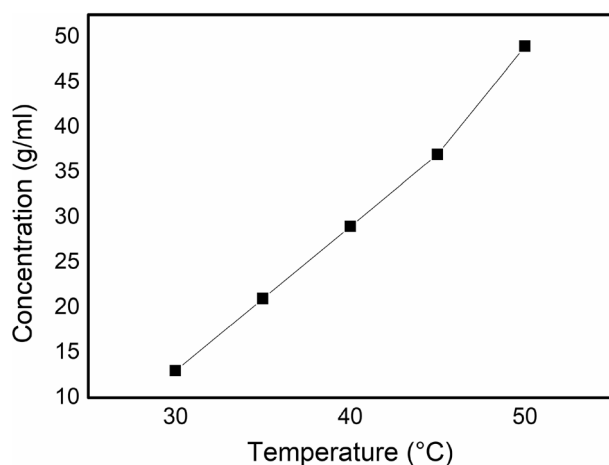


Fig. 2 Solubility curve of 2A6MP

temperature represent the positive solubility behavior.

3 Results and discussion

3.1 Single crystal XRD analysis

The physicochemical properties of the grown crystals are strongly depending on the crystal structure, symmetry, and lattice parameters. These materials properties are analyzed by single crystal X-ray diffractometer of Bruker Kappa APEX II. The results of crystal structure, bond lengths, bond angles, and tetrahedral parameters were estimated to the grown single crystals of 2A6MP. The entire structural reports were deposited to Cambridge Crystallographic Data Centre (CCDC) and the filed number is 2091828. The obtained results represented that the grown crystal was in monoclinic crystal structure with the centrosymmetric space group of $P12_1/c1$. The lattice parameters of 2A6MP crystal was, $a = 16.44(2) \text{ \AA}$, $b = 4.17(5) \text{ \AA}$, $c = 23.10(3) \text{ \AA}$, $\alpha = \gamma = 90^\circ$, $\beta = 107.84(4)^\circ$, and the unit cell volume of $V = 1508.7(3) \text{ \AA}^3$. The refined crystal structure data for 2A6MP are presented in Tables 1 and 2. The entire refinement data of 2A6MP crystal are given away in Supp. Tables 1–6. The thermal ellipsoid diagram of 2A6MP is presented in Fig. 3a which contains the asymmetric unit. It has mono *p*-chlorobenzoate anion, 2-amino-6-methylpyridinium cation with two water molecules. Also, the 2-amino-6-methylpyridinium cation and *p*-chlorobenzoate anion are linked through N–H...O hydrogen bond which the anion was

Table 1 Crystal data for 2A6MP

Identification code	2A6MP
Chemical formula	$C_{13}H_{17}ClN_2O_4$
Formula weight	300.74 g/mol
Temperature	303(2) K
Wavelength	0.71 \AA
Crystal size	0.21 × 0.26 × 0.32 mm
Crystal system	Monoclinic
Space group	$P 1 2_1/c 1$
Unit cell dimensions	$a = 16.44(2) \text{ \AA}$ $\alpha = 90^\circ$ $b = 4.17(5) \text{ \AA}$ $\beta = 107.84(4)^\circ$ $c = 23.10(3) \text{ \AA}$ $\gamma = 90^\circ$
Volume	$1508.7(3) \text{ \AA}^3$
Z	4
Density (calculated)	1.32 g/cm^3
Absorption coefficient	0.26 mm^{-1}
F(000)	632

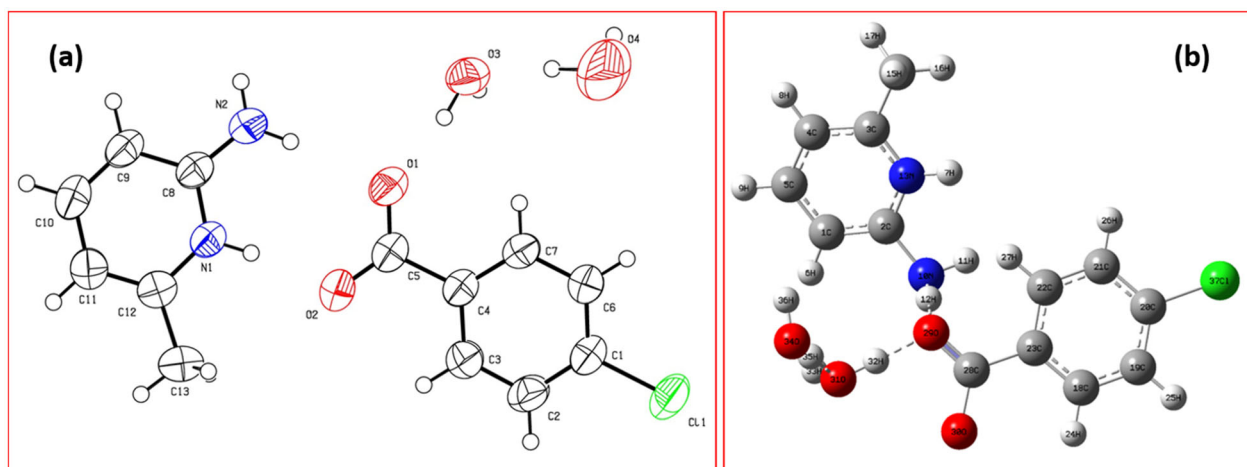
connected through water molecule of O–H...O hydrogen bond. Further, this water molecule was connected by another water molecule in the crystal structure through O–H...O hydrogen bond. It has been observed from the single crystal structural analyses, the three-dimensional structure of 2A6MP crystal was formed by the weak π – π interactions.

3.2 Molecular geometry

In molecular structural design, the hydrogen bond interactions are playing a major role. In this study, 2-amino-6-methylpyridine can act as a hydrogen acceptor moiety that easily bonds through *p*-chlorobenzoic hydrogen donor moiety. It can happen through N10–H12...O29 interactions which could imply the charge transfer between these moieties. The optimization of 2A6MP crystal structure was carried out from the single crystal XRD orped diagram is shown in Fig. 3b. The bond lengths and bond angles were calculated from the density functional theory (DFT) that values are compared with the experimental single crystal XRD data. The comparison is shown in Table 3. The theoretical values are slightly changed with the experimental values due to DFT estimations being made in the gaseous state while the experimental results were made in solid state. Hence, there shall be a minor deviation and could be observed as expected. The intermolecular interactions of 2A6MP crystal are indicated by dashed lines in Fig. 3b which corresponds to the stabilization of

Table 2 Data collection and structure refinement for 2A6MP

Theta range for data collection	2.57 to 30.11°
Index ranges	$-23 \leq h \leq 23, -5 \leq k \leq 5, -30 \leq l \leq 32$
Reflections collected	24,553
Independent reflections	4388 [$R(\text{int}) = 0.03$]
Coverage of independent reflections	99.1%
Absorption correction	Multi-Scan
Structure solution technique	direct methods
Structure solution program	SHELXT 2014/5 (Sheldrick, 2014)
Refinement method	Full-matrix least-squares on F^2
Refinement program	SHELXL-2018/3 (Sheldrick, 2018)
Function minimized	$\Sigma w(F_o^2 - F_c^2)^2$
Data/restraints/parameters	4388/0/196
Goodness-of-fit on F^2	1.06
$\Delta/\sigma_{\text{max}}$	0.01
Final R indices	2611 data; $I > 2\sigma(I)$, $R1 = 0.04$, $wR2 = 0.12$ all data, $R1 = 0.09$, $wR2 = 0.15$
Weighting scheme	$w = 1/[\sigma^2(F_o^2) + (0.05 P)^2 + 0.36 P]$ where $P = (F_o^2 + 2F_c^2)/3$
Largest diff. peak and hole	0.22 and $-0.28 \text{ e}\text{\AA}^{-3}$
R.M.S. deviation from mean	$0.03 \text{ e}\text{\AA}^{-3}$

**Fig. 3** **a** Thermal ellipsoid plot of 2A6MP crystal and **b** Molecular geometry of 2A6MP crystal

the grown three-dimensional crystal system. It represents the electrons flow that happens from 2-amino-6-methylpyridinium (hydrogen acceptor) cation to *p*-chlorobenzoate anion. This charge transfer mechanism leads to the nonlinearity of the grown crystal. The N–C–N bond angle value is about 120° which correlates the positive charge displacement of a nitrogen atom to a carbon atom. Overall, the carbon atom acquired the positive charge that gives rise to the 2-amino-6-methylpyridinium cation to form the stable crystal structure.

3.3 Powder XRD analysis

The Powder X-pert pro diffractometer with $\text{CuK}\alpha$ radiation was utilized to record powder X-ray diffraction patterns of the crystals powder sample. It provides information about crystallinity and phase purity of the grown 2A6MP crystal. The diffraction pattern was strongly dependent on the scattering intensity which includes scattering angle, energy, and polarization of the 2A6MP powder sample. Figure 4a revealed those high intense nature peaks which were occurred due to the high crystallinity of the organic 2A6MP powder material. The peaks were indexed

Table 3 Experimental and optimized geometry parameters of 2A6MP crystal computed by B3LYP/6–311 + + G (*d, p*) basis set

Bond length (Å)		
Geometric parameters	B3LYP/6–311 + + G(<i>d, p</i>)	Experimental values
C1–C2	1.38	1.37
C2–C3	1.39	1.38
C3–C4	1.39	1.38
C4–C7	1.39	1.37
C6–C7	1.39	1.38
C8–C9	1.42	1.40
C9–C10	1.36	1.35
C10–C11	1.39	1.39
C11–C12	1.36	1.35
C12–C13	1.51	1.49
C1–C6	1.38	1.37
C4–C5	1.52	1.50
N1–C12	1.38	1.36
N2–C8	1.32	1.32
N1–C8	1.37	1.34
O2–C5	1.25	1.24
O1–C5	1.26	1.26
C2–H1	1.08	0.93
C3–H2	1.08	0.93
C6–H4	1.08	0.93
C9–H6	1.08	0.93
C10–H9	1.08	0.93
C13–H7	1.09	0.96
C13–H5	1.09	0.96
C7–H3	1.08	0.93
C13–H13	1.08	0.96
N1–H1A	1.00	0.86
N2–H2A	1.09	0.86
N2–H2B	1.09	0.86
O3–H12	0.96	0.86
O3–H11	0.98	0.94
O4–H3A	1.19	1.08
C11–C1	1.76	1.74
Bond angles(°)		
Geometric parameters	Experimental value	B3LYP/6–311 + + G(<i>d, p</i>)
C11–C12–N1	118.94	118.18
C7–C4–C3	118.71	118.96
C11–C12–C13	124.60	125.57
C12–C11–C10	119.40	119.59
C10–C9–C8	119.42	120.26
C4–C7–C6	121.01	121.07
C7–C4–C5	121.41	121.80
C9–C10–C11	120.95	120.94
N1–C8–C9	117.96	116.23
C1–C2–H1	120.6	120.88
C4–C3–H2	119.4	119.81
C1–C6–H4	120.5	120.52
C6–C7–H3	119.5	119.57

Table 3 continued

Bond angles(°)		
Geometric parameters	Experimental value	B3LYP/6–311 + + G(d, p)
C8–C9–H6	120.3	120.82
C9–C10–H9	119.5	119.30
C10–C11–H10	120.3	120.44
C12–C13–H7	109.5	110.19
C3–C2–H1	120.6	120.97
C8–N1–C12	123.32	124.69
N2–C8–N1	118.67	120.37
C12–N1–H1A	118.3	117.81
C8–N2–H2B	120.0	120.06
H7–C13–H13	109.5	108.03
H7–C13–H5	109.5	108.02
C6–C1–C11	118.73	119.31
C2–C1–C11	119.90	119.32
O1–C5–C4	118.21	118.73
O2–C5–C4	117.56	116.52
O2–C5–O1	124.23	124.71
H11–O3–H12	97.0	95.87
H3A–O4–H3B	103.4	105.64
Dihedral angles(°)		
Geometric parameters	Experimental value	B3LYP/6–311 + + G(d, p)
C11–C1–C6–C7	– 179.63	– 179.92
C11–C1–C2–C3	179.84	179.50
C2–C3–C4–C7	– 0.20	– 0.29
C9–C10–C11–C12	0.40	0.41
C7–C4–C5–O2	– 175.31	– 173.72
C12–N1–C8–N2	– 178.92	– 178.86
N2–C8–C9–C10	179.63	179.93
N1–C8–C9–C10	– 0.10	0.11
C12–N1–C8–C9	0.80	0.86
C8–N1–C12–C13	178.39	178.68
C8–N1–C12–C11	– 0.9	0.86

using the PowderX program. The lattice parameters are calculated from this analysis and it is compared with the single crystal XRD data and it is shown in Table 4. It is approximately equal to each other.

3.4 FT-IR spectral analysis

FT-IR spectroscopy was utilized to determine the various functional groups in the chemical structure. They deliberated the large number of vibrational bands which represent each functional group of the

molecule. The FT-IR spectra of grown 2A6MP crystals were obtained using a Kimaya Engineers FT-IR spectrometer with the KBr pellet technique, as shown in Fig. 4b. In general, the hydrogen bond interaction was occurred between the acid and base groups. The vibrational band at 3311 cm^{-1} was attributed to the N–H symmetric stretching which represents the nitrogen protonation of the pyridinium moiety [27]. The asymmetric and symmetric stretching vibrations are occurred at $2919, 2840\text{ cm}^{-1}$. The C–H stretching

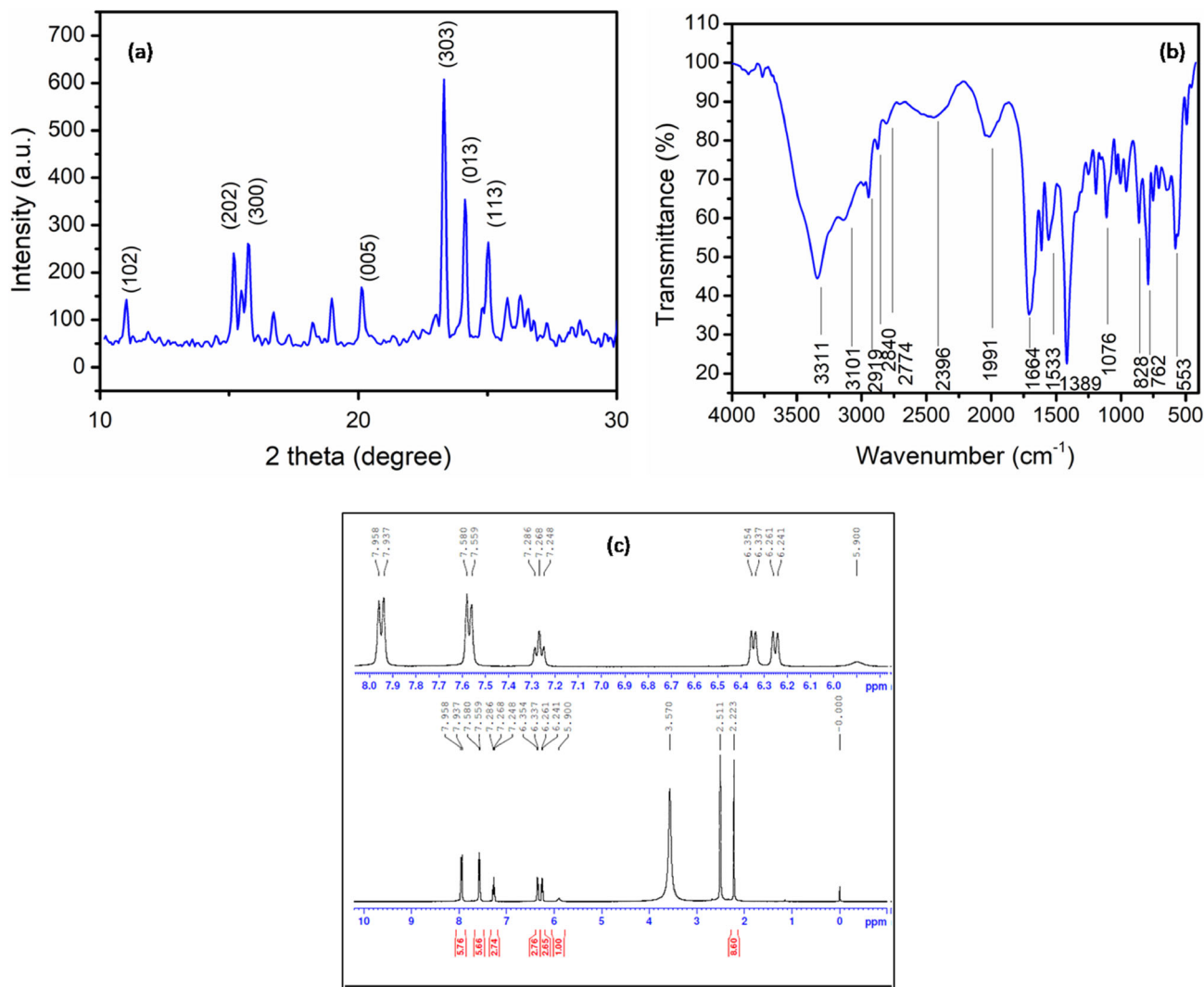


Fig. 4 **a** Powder X-ray diffraction pattern, **b** FTIR spectrum, and **c** NMR spectrum of 2A6MP crystal

Table 4 Comparison the lattice parameters of powder XRD with single crystal XRD

Powder XRD	Single crystal XRD
$a = 16.24 \text{ \AA}$	$a = 16.44(2) \text{ \AA}$
$b = 4.14 \text{ \AA}$	$b = 4.17(5) \text{ \AA}$
$c = 23.09 \text{ \AA}$	$c = 23.10(3) \text{ \AA}$
$\alpha = 90.03^\circ$	$\alpha = 90^\circ$
$\beta = 107.44^\circ$	$\beta = 107.84(4)^\circ$
$\gamma = 90.05^\circ$	$\gamma = 90^\circ$

of methyl (CH₃) group in pyridinium moiety was confirmed by the vibrational band at 2724 cm⁻¹. The bands are broadly in the region of 2500–3500 cm⁻¹ is due to the O–H stretching vibration. The C–H

stretching for the benzene ring was associated with the bands at 2396, 1991 cm⁻¹. The bands are at 1664, 1389 cm⁻¹ was ascribed to the asymmetric, symmetric COO⁻ stretching vibrational frequency of the carboxylic group in the *p*-chlorobenzoate anion. The C=C stretching vibration occurred at 1533 cm⁻¹. The vibrational band at 1076 cm⁻¹ corresponds to the O–H in-plane bending vibration [28]. C–N–O in-plane bending, C–N–C out of plane bending are assigned to the vibrational bands at 828, 553 cm⁻¹, respectively. The band occurred at 762 cm⁻¹ was due to the C–Cl vibrational stretching frequency of the *p*-chlorobenzoate anion [29]. The hydrogen bond interactions were confirmed by the N–H and O–H stretching vibrations. The assigned complete vibrational bands are presented in Table 5.

Table 5 FT-IR spectral vibrational assignments of 2A6MP compound

FTIR (cm ⁻¹)	Assignments
3311	N–H symmetric stretching
3101	C–H stretching vibration
2919	CH ₃ asymmetric stretching
2840	CH ₃ symmetric stretching
2724	CH stretching of CH ₃
2396, 1991	C–H stretching vibration
1664	Symmetric stretching of COO ⁻ group vibration
1533	C=C stretching vibration
1389	Asymmetric stretching of COO ⁻ group vibration
1076	O–H in-plane bending
828	C–N–O in-plane bending vibration
762	C–Cl stretching vibration
553	C–N–C out of plane bending

3.5 ¹H NMR spectral analysis

The Bruker Avance III HD Nano Bay 400 MHz FT-NMR spectrometer was used to analyze the ¹H NMR spectrum of 2A6MP crystal at room temperature using the standard reference of deuterated solvent DMSO₄, and the spectrum was displayed in Fig. 4c. The CH₃ proton of pyridinium moiety was confirmed through the sharp singlet peaks at $\delta = 2.22$ and 2.51 ppm. The singlet proton signal was seen at $\delta = 3.57$ ppm which indicates the NH₂ proton of pyridinium moiety. The doublet of doublet proton signals occurred in the range of 6.24–6.35 ppm and the triplet proton signals from 7.25 to 7.29 ppm which corresponded to the two-hydrogen benzene ring in pyridinium moiety. The presence of proton signal at 5.90 ppm was due to the CH proton of benzoate anion moiety. The doublet proton signal exhibited at $\delta = 7.58$ and 7.56 ppm were represented the two hydrogens of benzene ring in benzoate moiety. Also, the doublet of doublet signals was viewed in the NMR spectrum at 7.94 and 7.96 ppm which were pointed out the two protons of the benzene ring in benzoate moiety [30].

3.6 UV–Vis spectral analysis

UV–Vis spectral analysis recognizes the cut-off wavelength and optical transparency of the grown 2A6MP crystal using Ocean Optics HR 2000 spectrometer. These parameters are important to the parametric oscillations and nonlinear optical

applications etc. [31]. UV–Vis transmission, absorption spectral analyses were revealed in Fig. 5a, b. It elaborately gives the 2A6MP electronic transitions. When the UV region absorbs the light, the electrons are moving from the lower (ground) to the upper states in the orbitals of σ and π . The grown crystal attained the lower cut-off at 349 nm (UV region) and good optical transparency in the visible region of 66% as revealed in Fig. 5a ensured the grown crystal nonlinearity. Also, the light absorbance does not happen between 400 and 1100 nm and it indicates that the grown crystals are defects free. The bandgap was estimated from Tauc's plot which correlates the optical absorption coefficient (α) and $h\nu$ (photon energy). These parameters are calculated from the optical absorption spectra (Fig. 5b). The ' α ' was calculated by the following relation,

$$h\nu\alpha = A(h\nu - E_g)^{1/2}, \quad (1)$$

' E_g ' represents the bandgap, ' A ' indicates an invariable. The graph is plotted between the value of $(\alpha h\nu)^2$ vs. $h\nu$ and denoted as Tauc's plot. The linear part of this plot is to identify the band gap of the grown crystal as shown in Fig. 5c and the band gap was found to be about 3.19 eV. The significant transmittance in the visible range is confirmed by the 2A6MP crystal's wide band gap, and defect concentration is lower in the grown crystal. The pyridinium derivative single crystals attained the wide bandgap [26, 32, 33] are compared with the present work and it is shown in Table 6. The lower cut-off and wide band gap ensured the grown 2A6MP crystal can be used for optoelectronic applications.

3.7 PL spectral analysis

PL spectral study is one of the most fascinating methods to find out the luminescence behavior such as excitation and emission spectrum of grown organic crystals. The Varian Cary Eclipse photoluminescence spectrometer was used for the experiment. Hence, a high emission peak in the fluorescence represents the grown material is imperative in the field of optoelectronic applications [34, 35]. The PL spectrum was recorded for the grown 2A6MP material in the wavelength range from 300 to 600 nm as shown in Fig. 5d. The high intense broadening peak was occurred at 378 nm in the violet region because of their 2-amino-6-methylpyridinium

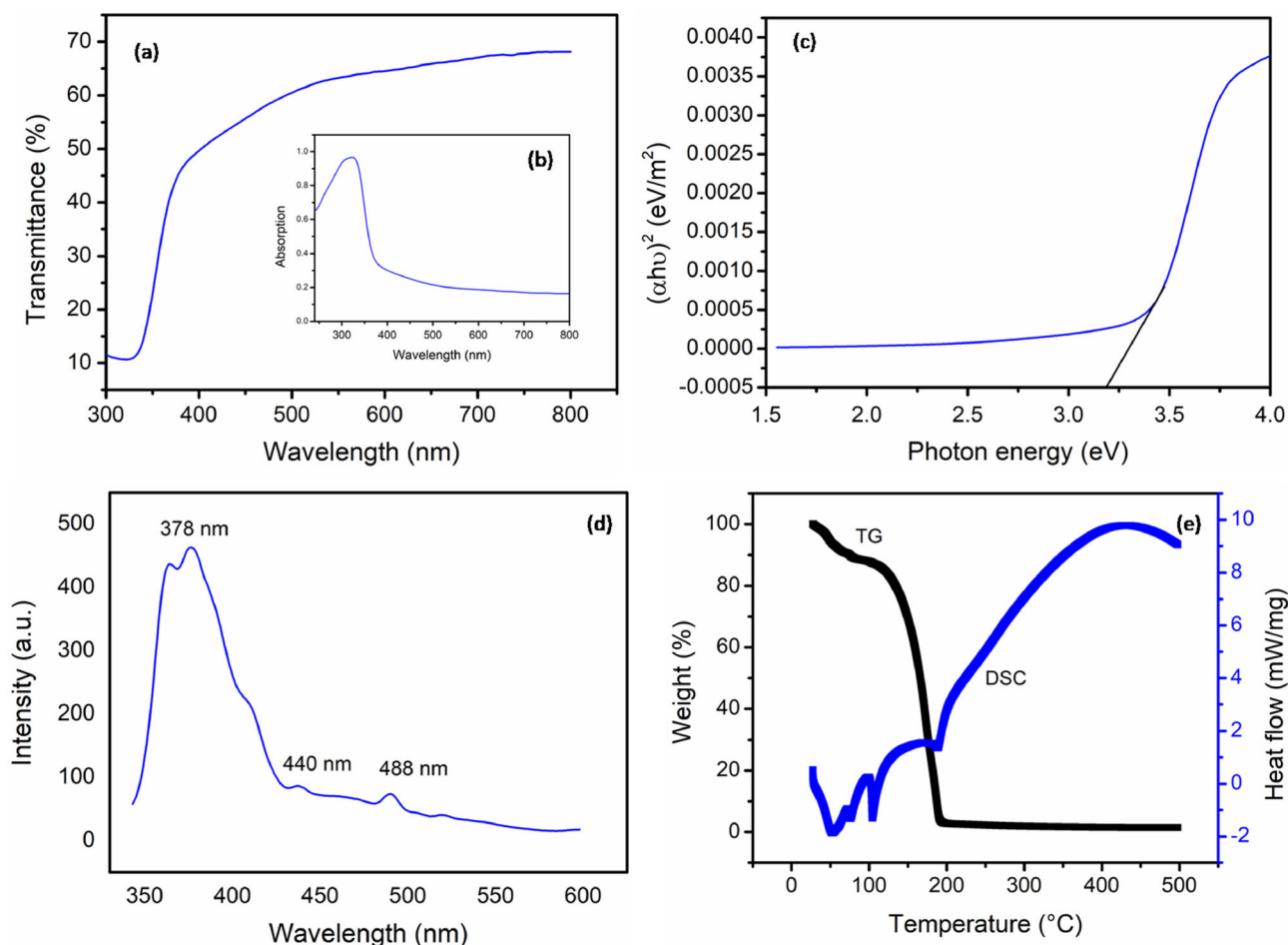


Fig. 5 **a, b** UV–Vis transmittance and absorbance spectrum, **c** Tauc's plot, **d** Photoluminescence spectrum, and **e** TG-DSC curve of 2A6MP

Table 6 Comparison of pyridinium derivative crystals band gap with the present work

Pyridinium derivative crystals	Band gap (eV)
2A6M4N [26]	3.42
2APS [32]	3.45
2A6MPS [33]	3.35
Present work (2A6MP)	3.19

cation ions are excited into the first electronic excited state (higher vibrational) subsequently to the lowest single excited state with the excitation wavelength at 348 nm. At the particular state, the electrons are released to the ground state with luminescence emission simultaneously. The intense peak regarding the proton interchanges between 2-amino-6-methylpyridinium and *p*-chlorobenzoate ions. The low intensity peaks at 440 and 488 nm are attributed

to the hydrogen bond in the crystal lattice. It indicates that a 2A6MP crystal has a blue light emission. This results show that 2A6MP crystal may have suitable application in the violet and blue emit diodes.

3.8 TG-DSC analysis

Thermogravimetric (TG) and differential scanning calorimetric (DSC) analysis were performed on 1.5 mg mass of powdered 2A6MP crystal sample and was taken over the alumina crucible, when the temperature varied from 30 to 500 °C at the heating rate of 10 °C/min in the nitrogen atmosphere to investigate the melting point, thermal stability, and decomposition point of the grown crystal by using DSC-SDT-Q600. Thermal stability is one of the important characteristics to find out the fabrication of device oriented applications [36]. TG-DSC curve for the grown 2A6MP crystal is shown in Fig. 5e. From

the TG curve, weight loss has occurred when the temperature reached to 106.9 °C and the material was stable below this temperature. After that, the heavy weight loss was observed at the temperature of 192.8 °C indicates most of the volatile substances are released from the grown crystal. The DSC curve exhibits the first endothermic peak at 106.9 °C which represents the dehydration of the 2A6MP crystal and the second endothermic peak of the DSC curve at the temperature of 193.87 °C indicates the decomposition of the grown crystal. From this analysis, the 2A6MP crystal was found to be a useful candidate for the NLO and laser applications up to the temperature rate at 106.8 °C.

3.9 Microhardness analysis

Microhardness analysis, which is the characteristic of mechanical properties of any grown crystal, that is related to the properties of physical and chemical directly related to the device fabrication applications [37]. 2A6MP crystal hardness measurement was done by Vickers's micro hardness tester. When the load was applied from 5 to 100 g on the grown 2A6MP crystal, the hardness number was calculated by using this relation [38],

$$H_v = 1.8544 \times \frac{P}{d^2} \text{ kg/mm}^2, \quad (2)$$

where ' H_v ' represents the hardness number, ' P ' denotes the functional load in kg, ' d ' is diagonal length of the indenter in mm, 1.8544 is a geometrical constant factor. When the load was applied to the 2A6MP crystal up to 50 g the hardness number was increased, and it is shown in Fig. 6a after that the cracks were induced. At the higher loads, the indentation stress was released to the material. As it follows the material undergoes elastic recovery. Figure 6b revealed the plotted graph between the functional loads versus diagonal length indentations. The increasing of hardness number with respect to the load denotes the reverse indentation size effect (RISE) [39]. Functional load and indenter diagonal length are interconnected by Meyer's law as follows [40],

$$P = Ad^n, \quad (3)$$

here ' n ' refers the work hardening co-efficient or Meyer's index of the grown crystal. With the result of Onitsch [41], the Meyer's index range was about 1 to 1.6 for harder materials and above 1.6 identical into

the soft material family. The graph is drawn between $\log P$ vs. $\log d$ as shown in Fig. 6(c) to find the value of ' n '. From this graph, the value of Meyer's index was found to be about 2.84 hence the grown crystal was classified into the soft material category. If $n < 2$ indicates normal ISE behavior, $n > 2$ reveals the behavior of reverse ISE. Thus, the grown 2A6MP crystal belongs to reverse ISE behavior. The important parameters of Yield strength [42] and Stiffness constant [43] of 2A6MP crystal were calculated from the following empirical formula,

$$\sigma_y = \frac{H_v}{2.9} \left[1 - (n - 2) \frac{12.5(n - 2)}{1 - (n - 2)} \right]^{n-2}, \quad (4)$$

$$C_{11} = H_v^{(7/4)}. \quad (5)$$

The plot is drawn between identical load (P) and Yield strength of 2A6MP crystal as revealed in Fig. 7a. The identical load vs. stiffness constant was plotted and shown in Fig. 7b. The values of Stiffness constant and Yield strength were increased with respect to the identical loads. These are the essential key factors for the materials structure as well as bonding [44] of crystal structure that was used for materials science engineering. The high magnitude of hardness number, Yield strength, and Stiffness constants were shown in Table 7 that strongly evidenced for 2A6MP crystal to be used as NLO material. Compared with the other pyridinium derivative single crystal, the grown crystal exhibits the good mechanical strength [26, 32, 33].

3.10 Frontier molecular orbital (HOMO – LUMO) analyses

Frontier molecular orbital includes both HOMO (highest occupied molecular orbital) and LUMO (lowest unoccupied molecular orbital). The excitation of electrons from HOMO–LUMO orbitals describes the transition of electrons that commence from the ground state (electronic absorption) toward first excited state (electronic transition) [45]. HOMO represents an electron donor and LUMO indicates an electron acceptor which implies that electron density is transferred between these orbitals. In this grown crystal structure, HOMO of 2A6MP is delocalized over the *p*-chlorobenzoate anion, LUMO is spread over the 2-amino-6-methylpyridinium cation as shown in Fig. 8 which is responsible for the electron density transfer from anion to cation. As of Fig. 8, the

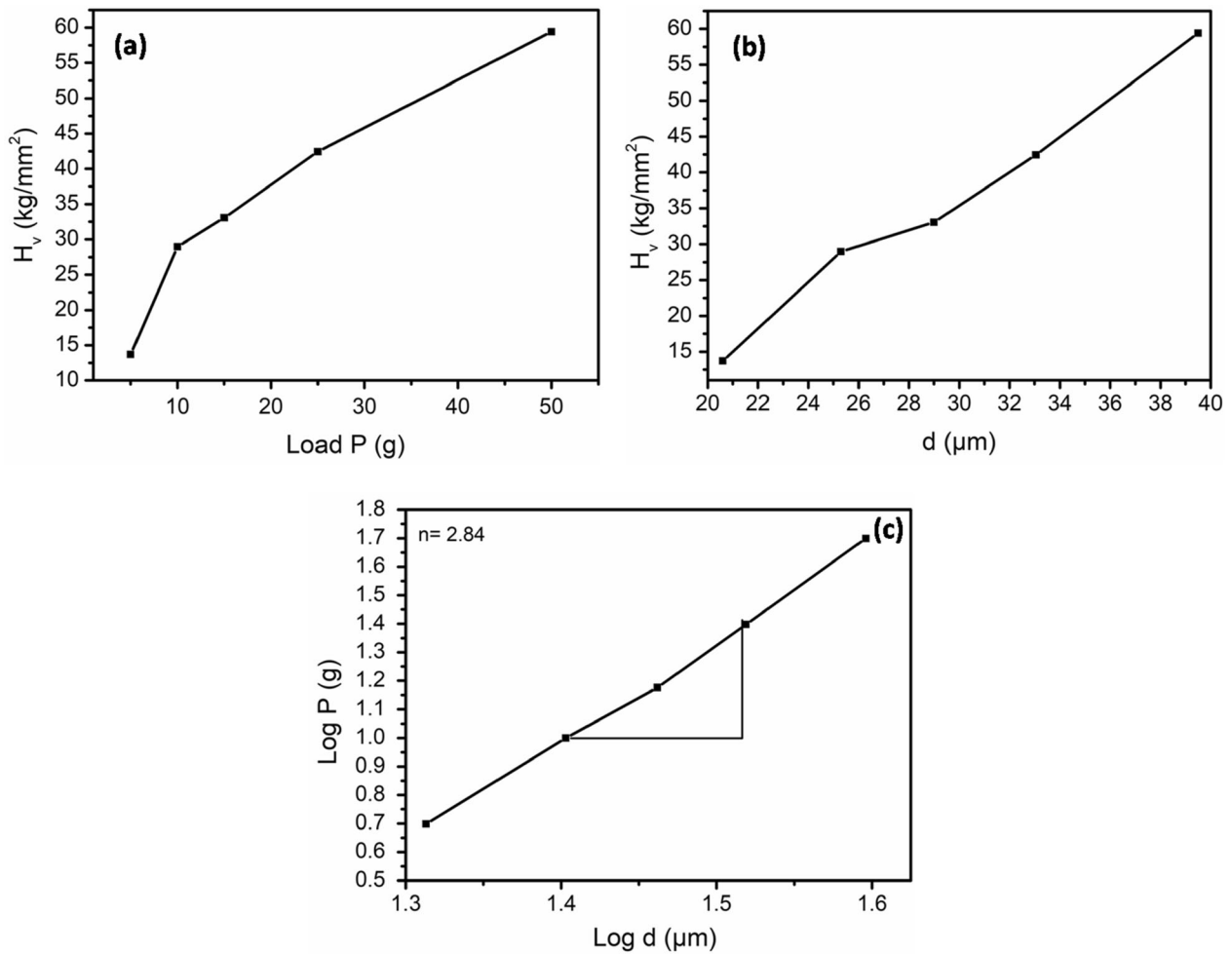


Fig. 6 Plot of **a** Hardness number (H_v) vs. load (P), **b** H_v vs. diagonal (d) and **c** $\log P$ vs. $\log d$

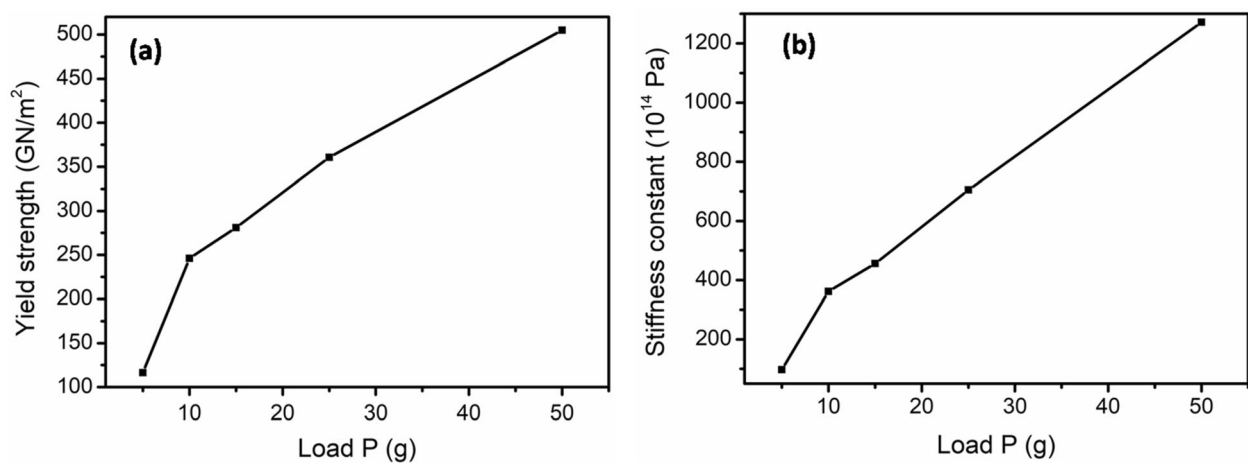


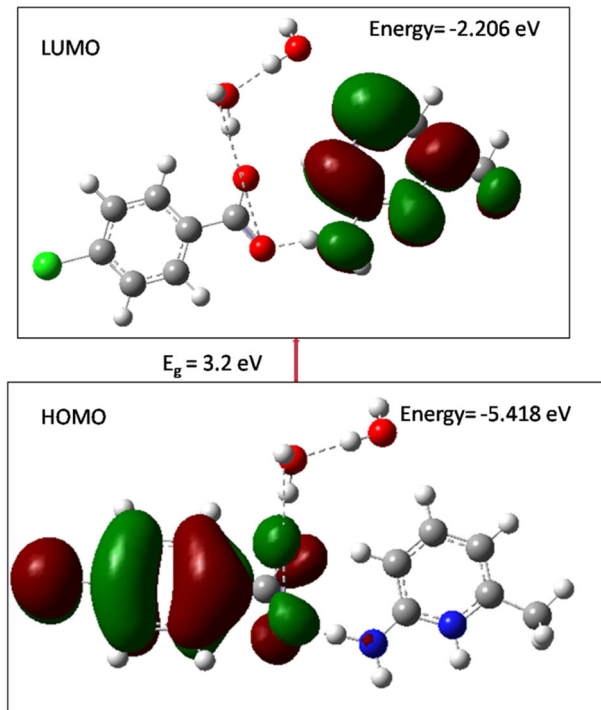
Fig. 7 Plot of **a** Yield strength (σ_y) vs. load P and **b** Stiffness constant (C_{11}) vs. load P

red color covered the positive region, and the green color occupied the negative region of 2A6MP. The

HOMO, LUMO energies are calculated with the same level of theory. The difference between HOMO and

Table 7 Microhardness (H_V), Yield strength (σ_y), Stiffness Constant (C_{11}) for different loads

Load P (g)	H_V (kg/mm ²)	Meyer's Index (n)	σ_y (GN/m ²)	$C_{11} \times 10^{14}$ (Pa)
5	13.71	2.84	116.5	97.68
10	28.96	2.84	246.1	361.53
15	33.06	2.84	280.9	455.80
25	42.43	2.84	360.5	705.38
50	59.41	2.84	504.8	1271.31

**Fig. 8** Molecular orbitals of HOMO and LUMO

LUMO energy gives the band gap, which is the crucial part of the 2A6MP crystal. It gives electrical

Table 8 HOMO–LUMO energy gap and their related molecular properties of 2A6MP molecule

Molecular properties (B3LYP/6-311G + + (d, p))	
HOMO _{energy}	– 5.41 eV
LUMO _{energy}	– 2.20 eV
HOMO-LUMO _{energy gap}	3.21 eV
Ionization potential (I)	5.41 eV
Electron affinity (A)	2.20 eV
Chemical hardness (η)	1.60 eV
Reciprocal of hardness (S)	0.62 eV
Chemical potential (μ)	– 3.81 eV
Electro negativity (χ)	3.81 eV
Electrophilicity (ω)	4.52 eV

properties, stabilization of the entire crystal structure also evidenced for charge transfer occurred between these molecules. Using the HOMO, LUMO energies, the following factors are calculated and the values are revealed in Table 8.

$$\text{Ionization potential } (I) = -\text{Homo energy}, \quad (6)$$

$$\text{Electron affinity } (A) = -\text{Lumo energy}, \quad (7)$$

$$\text{Chemical hardness } (\eta) = (I - A/2), \quad (8)$$

$$\text{Global softness } (S) = 1/(\eta), \quad (9)$$

$$\text{Chemical potential } (\mu) = -(I + A/2), \quad (10)$$

$$\text{Electro negativity } (\chi) = (I + A/2), \quad (11)$$

$$\text{Electrophilicity } (\omega) = \mu^2/2\eta. \quad (12)$$

HOMO energies are directly connected with ionization potential and the LUMO energies are linked with electron affinity [46]. Chemical hardness and softness are related to the material stability of the 2A6MP crystal. Sharing of electrons was focused by the electrons represented the electro negativity and the electrons are recognized from the donor group assigned to an electron affinity. The energy gap of 2A6MP crystal is about 3.21 eV.

3.11 Molecular electrostatic potential

Molecular electrostatic potential (MEP) mapping is an essential technique to provide information about atomic, molecular properties also net electrostatic effect produced by the overall charge distribution of the entire molecule at a space point. The 2A6MP molecules nucleophilic and electrophilic reaction sites are represented by the various colors in the order of red < orange < yellow < green < blue. The electrostatic potential map closed and open curvature shown in Fig. 9a, b was derived from the optimization of the 2A6MP crystal structure using the same B3LYP theory, which also aids in the analysis of 2A6MP intermolecular interactions. The electrophilic site is susceptible to electron withdrawing with MEP

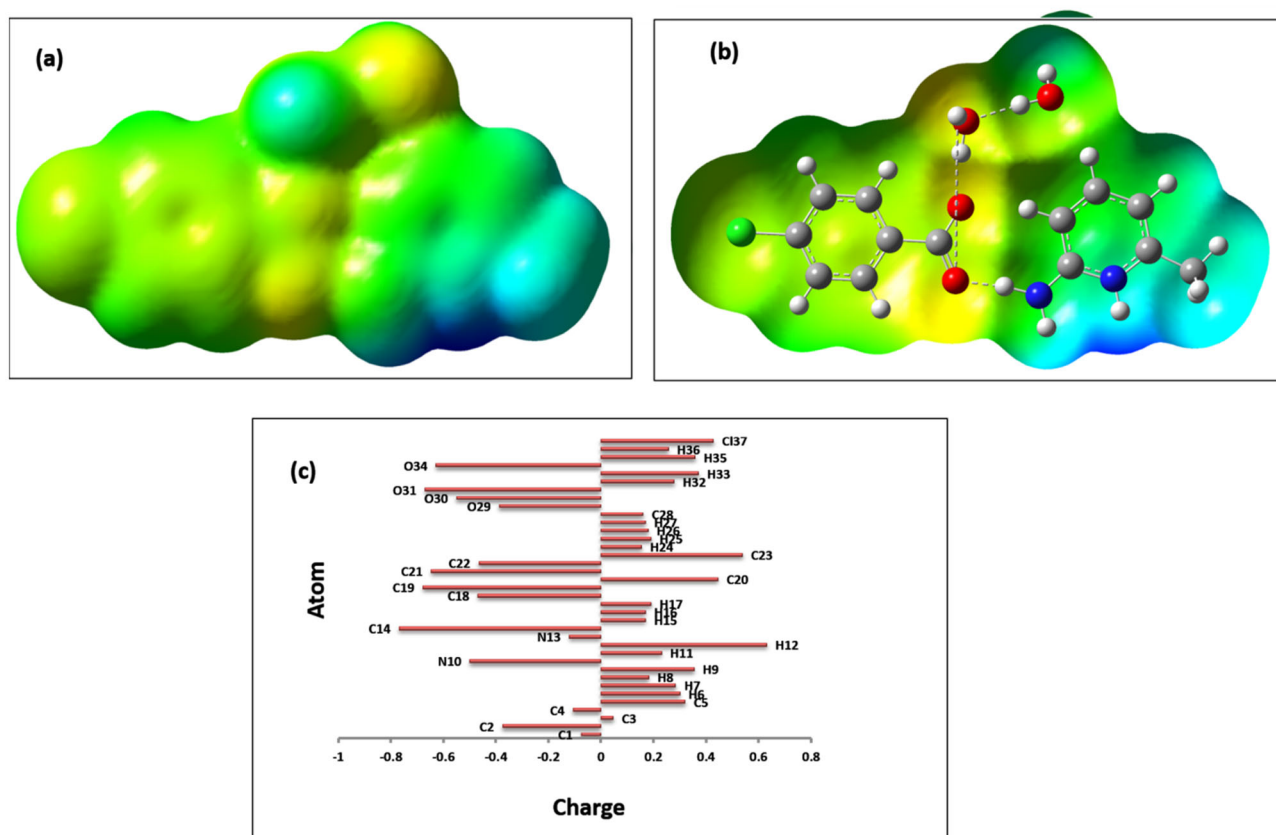


Fig. 9 Plot of **a** closed **b** opened molecular electrostatic potential and **c** Mulliken analysis of 2A6MP crystal

minima and the nucleophilic site predicts the electron deficient with high MEP. The electrostatic negative potential region is presented in the carboxyl oxygen group of benzoate anion as revealed in yellow color indicates that the oxygen atoms can act as an electrophilic site which are highly surrounded by the positive charge. The electrostatic positive potential region marked by the blue color, which is located at the hydrogen atom of nitrogen, amino group pyridinium cation represented the nucleophilic site. Hence the intermolecular interactions are formed between these molecules by N–H...O hydrogen bond interaction. It includes both theoretical and experimental single crystal data analysis on the N–H...O hydrogen bond interactions inside the 2A6MP molecule. As a result, the charge transfer that happens within the 2A6MP molecule between the anion and cation molecule demonstrated good NLO response.

3.12 Mulliken charge analysis

Mulliken charge distribution analysis manipulates the polarizability, and the dipole moment changes between the chemical bonds. The amount of charge distribution in the 2A6MP crystal structure was calculated and its graphical visualization of atomic charges is given in Fig. 9c. The highest negative charge exhibits the oxygen of O29, O30 carboxyl groups of benzoate moiety and the significant positive charge over the hydrogen atom of H12, H32, H33, and H36 of pyridinium moiety compared with other hydrogen atoms of benzene ring that strong evidence for the N–H...O intermolecular interactions of hydrogen bond between the benzoate and pyridinium moiety. Compared with all other carbon atoms, C19 possessed a maximum positive charge due to the occurrence of electronegative atoms. The electronegative atoms such as nitrogen, oxygen possessed a negative charge. This analysis also supports the claim of electrophilic and nucleophilic sites as well as MEP. The charge transfer between the anion

and the cation within the 2A6MP molecule was also confirmed which resulted in nonlinearity.

3.13 NBO

The existence of inter and intramolecular hydrogen bond interactions of 2A6MP was analyzed from NBO analysis [47]. It helps to understand the possible hydrogen interactions between Lewis (filled) and non-Lewis (unfilled) molecular systems with detail to the hydrogen donor and an acceptor. Second order Fock matrix calculations were tabulated in Supp. Table 7. The lone pair oxygen atom in the bonding orbital was strongly hydrogen bonded into the antibonding N–H through N10-H11...O29 and N10-H12...O29 interactions, due to these interactions the transportation of charges from bonding to antibonding existence of the hydrogen donors through the stabilization energies 0.08 and 27.77 kcal/mol, respectively. The electron density was enhanced by 0.01 in these interactions strongly denoted that both bonds are weakening. It is revealed that the strong hydrogen bond interactions of N–H...O into the oxygen atom of benzoate yielded the molecular stability of the 2A6MP molecule. Pyridinium acted as a hydrogen bond acceptor that easily bonded through the oxygen atom of benzoate representing the charge transfer between these molecules. This process leads to be, the molecule has exceedingly polarized. Hence the 2A6MP shall be responsible for the enhanced NLO properties.

3.14 Z-scan

One of the most important technological experimental approaches is the phenomenon of four waves mixing, which symbolizes third-order nonlinearity. It is related to the intensity dependent refraction and absorption which are used in the field of photonic devices development such as optical signal processing applications. Therefore, the third-order nonlinearity measurement was of vital importance. Z-scan method using He–Ne laser source is the simple implemented technique used a single beam and gives the information about the nonlinear susceptibility of both real and imaginary parts as well as nonlinearity. The open aperture measurement mode detailed the nonlinear absorption co-efficient and the closed aperture gives us information about nonlinear refractive index [48] of grown 2A6MP crystal.

The closed aperture curve is shown in Fig. 10a and revealed the transmittance of peaks are lowered to valley indicated the self-defocusing nature, i.e., nonlinear refractive index [49] attained the negative sign. The variation of refractive index with respect to the temperature is called self-defocusing. The nonlinearity sign is essential parameter of optical signal applications. Figure 10b depicts the open aperture curve for 2A6MP crystal that exhibits the high intensity near the focus named saturable absorption. The phenomenon of saturable absorption is when the excited molecules directly decay back to the ground state due to the high transmittance and the reduction of focal points [50]. The nonlinear absorption co-efficient (β) was intended by the following equation,

$$\beta = \frac{2\sqrt{2\Delta T}}{I_o L_{eff}} \text{ (m/W)}, \quad (13)$$

where ΔT - peak value from the OA curve. I_o represents the input intensity. L_{eff} indicates the thickness of the crystal sample; L_{eff} can be deliberated by the following relation,

$$L_{eff} = 1 - e^{-\alpha L/\alpha}, \quad (14)$$

where ' α ' and ' L ' denotes the linear absorption coefficient and sample thickness of the grown 2A6MP crystal. The value of n_2 was calculated by using the below relation,

$$n_2 = \frac{\Delta\phi}{KI_o L_{eff}}, \quad (15)$$

here $\Delta\phi$ represents the phase shift axis at the focus and it was calculated by the following relation,

$$\Delta\phi = \frac{\Delta T_{p-v}}{0.406(1-S)^{0.25}}, \quad (16)$$

' S ' indicates the linear transmittance, which was deliberated by the following equation,

$$S = 1 - \exp\left(\frac{-2r_a^2}{w_a^2}\right), \quad (17)$$

here the value of ' r_a ' is (radius of aperture) = 1.25 mm; and ' w_a ' (beam radius) is = 3.25 mm. The real part of 2A6MP crystal third-order nonlinear optical susceptibility (χ^3) was calculated by

$$R_e\chi^{(3)} = \frac{10^{-4}\epsilon_o C^2 n_2 n_o^2}{\pi}, \quad (18)$$

and.

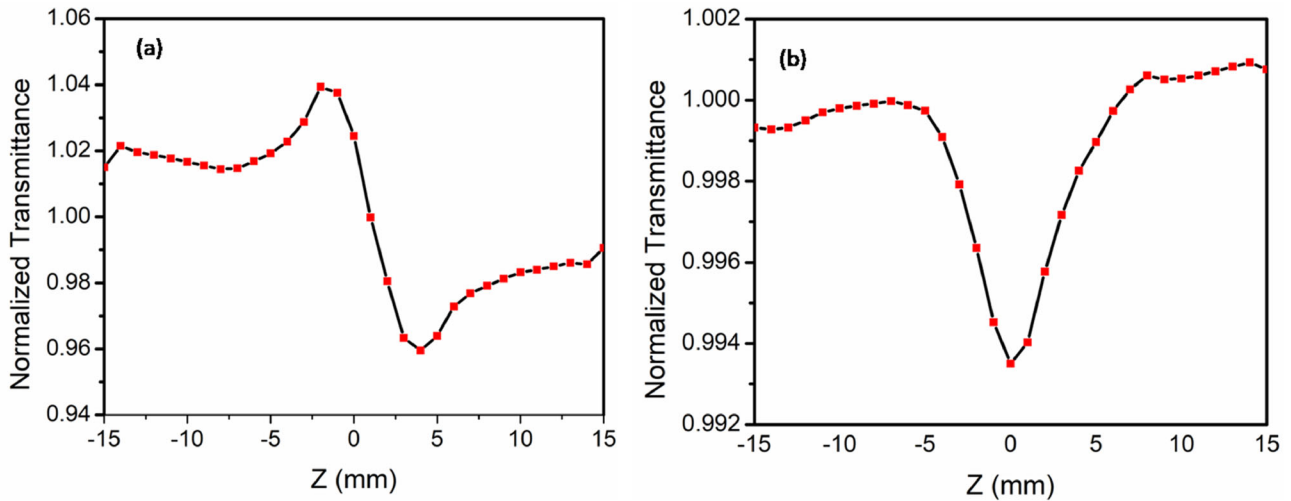


Fig. 10 a closed b opened aperture Z-scan analysis of 2A6MP crystal

The Imaginary part was estimated by

$$I_m\chi^{(3)} = \frac{10^{-2}\epsilon_0 C^2 \lambda \beta n_0^2}{4\pi^2} \tag{19}$$

The $\chi^{(3)}$ of 2A6MP crystal was calculated by using Eq. (18) & (19)

$$\chi^{(3)} = \sqrt{\{R_e(\chi^{(3)}) + I_m(\chi^{(3)})\}^2} \tag{20}$$

The value of nonlinear refractive index (n_2) and nonlinear absorption coefficient (β) is found to be $-4.25 \times 10^{-09} \text{ m}^2/\text{W}$ and $3.16 \times 10^{-04} \text{ m/W}$ from the closed and open aperture curve, respectively. The third-order susceptibility (χ^3) was calculated using these parameters and found to be $4.95 \times 10^{-06} \text{ esu}$. The high magnitude of third-order susceptibility represented that the intermolecular interactions of the grown crystal due to the polarization of the

molecular system. The grown crystal attained the self-defocusing behavior and has good agreement results which can have NLO applications. The other familiar NLO crystals nonlinear refractive index, nonlinear absorption co-efficient, and third-order susceptibility are compared [51–55] with the present work as shown in Table 9. Compared with the other NLO crystals the grown 2A6MP crystal exhibits high third-order nonlinear response.

4 Conclusion

The organic single crystal of 2-amino-6-methylpyridinium *p*-chlorobenzoate dihydrate (2A6MP) was grown by solution growth technique of slow evaporation method. Single crystal XRD analysis was revealed the structural parameters that evidenced the

Table 9 Comparison of some familiar NLO crystals nonlinear refractive index, nonlinear absorption co-efficient, and third-order susceptibility

Sample	Nonlinear refractive index(n_2) cm^2/W	Nonlinear absorption co-efficient (β) cm/W	Third-order susceptibility(χ^3) esu
2A6MP4HB [51]	-5.61×10^{-12}	5.08×10^{-6}	8.35×10^{-10}
2A6M2H [52]	4.68×10^{-8}	0.17×10^{-3}	1.48×10^{-7}
2A4MP4MB [53]	6.50×10^{-8}	0.02×10^{-4}	3.14×10^{-6}
Pure ADP [54, 55]	6.34×10^{-11} 2.85×10^{-10}	9.55×10^{-6} 5.51×10^{-6}	1.73×10^{-5} 1.18×10^{-5}
2A6MP [present work]	-4.25×10^{-9}	3.16×10^{-4}	4.95×10^{-6}

ICT mechanism of 2A6MP molecular system. The presence of NH and OH groups were observed from FT-IR confirmed the ICT mechanism of 2A6MP crystal. The UV–Vis optical studies of 2A6MP crystal revealed the cut-off wavelength of 349 nm in the UV region and good transmittance of about 66% in the visible region. Thermal analysis showed that the grown 2A6MP crystal was thermally stable up to the temperature rate of 106.8 °C. Vickers's hardness analysis identifies that the grown crystal goes into the soft material category with a high value of hardness, Yield strength, and Stiffness constant ensured the grown crystal which is suitable for NLO applications. Z-scan analysis revealed that third-order nonlinear response of the grown crystal such as nonlinear susceptibility $\chi^3 = 4.95 \times 10^{-06}$ esu. DFT studies were also confirmed that the 2A6MP crystal has an ICT transfer mechanism that induced the nonlinear property theoretically. Overall the title crystal is well suitable for optoelectronic applications.

Acknowledgements

Authors acknowledge that this article has been written with the financial support of RUSA-Phase 2.0 grant sanctioned vide Letter No.F.24-51/2014-U, Policy (TNMulti-Gen), Dept.of Edn. Govt. of India, Dt.09.10.2018. Also, the authors express their thanks to DST-PURSE-II New Delhi, UGC-SAP, DST-FIST and Alagappa University, Karaikudi-03, Tamil Nadu, India for their encouragement and providing excellent facilities.

Authors' contribution

RK: conceptualization, investigation, writing—original draft. GP: formal analysis, resources. GR: validation, VMK: methodology, software. MKK: writing—review and editing, validation. SS: project administration, supervision, writing—review and editing.

Data availability

The data that support the findings of this study are available within the article.

Declarations

Conflict of interest The authors declare that they have no conflict interest.

Humans and animals statement This article does not contain any studies involving humans and animals performed by any of the authors.

Supplementary Information: The online version contains supplementary material available at <http://doi.org/10.1007/s10854-021-07650-3>.

References

1. C. Bosshard, K. Sutter, P. Prêtre, J. Hulliger, M. Flörsheimer, P. Kaatz, P. Günter, Organic nonlinear optical materials, CRC press, (2020)
2. D.S. Chemla, J. Zyss, Nonlinear Optical Properties of Organic Molecules and Crystals VI. Academic Press, 1, (2012)
3. R. Anbarasan, J. Kalyana Sundar, Experimental and quantum chemical investigation on imidazolium trifluoroacetate single crystal for optoelectronic applications. *J. Mater. Sci. Mater. Electron.* **30**, 10224–10232 (2019)
4. R. Anbarasan, P. Eniya, J. Kalyana Sundar, Experimental and quantum chemical investigation on piperazinium hexachloro stannous trihydrate single crystal for second harmonic generation applications. *J. Electron. Mater.* **48**, 7686–7695 (2019)
5. K. Thanigaimani, N.C. Khalib, S. Arshad, I.A. Razak, P. Sivajeyanthi, Molecular and crystal structure of two organic acid-base salts from 2-amino-6-methylpyridine and meta and para methylbenzoic acids. *Mol. Cryst. Liq. Cryst.* **607**, 156–168 (2015)
6. R. Anbarasan, E. Palaniyasan, A. Muppudathi, K. Jeyaperumal, Experimental and quantum chemical investigations of 4-bromoanilinium hydrogen phthalate crystal for optoelectronic applications. *Mater. Res. Express* **6**, 095105 (2019)
7. T. Sivakumar, P. Eniya, J. Kalyana Sundar, A. Thirunavukkarasu, M. Anna Lakshmi, G. Kanthimathi, Investigation on the Effects of MnCl₂ Doping on Structural and Optical Properties of DAST Single Crystals as Materials for Second Order Nonlinear Optics. *Cryst. Res. Technol.* **56**, 2100016 (2021)
8. T. Sivakumar, M. Anna Lakshmi, R. Anbarasan, P. Eniya, S. Vignesh, J. Kalyana Sundar, Exploring the influence of CdCl₂ on the nonlinear properties of 4-N, N-dimethylamino-4-N-methyl-stilbazolium tosylate (DAST) crystal for optoelectronic applications. *Mater. Technol.* 1–13, (2021)
9. T. Suthan, N.P. Rajesh, C.K. Mahadevan, G. Bhagavanarayan, Studies on crystal growth and physical properties of

- 2-amino-5-chloropyridine single crystal. *Mater. Chem. Phys.* **129**, 433–438 (2011)
- L. Jothi, K. Ramamurthi, Growth and characterization of an organic NLO crystal: 4-chloro-4-methyl benzylidene aniline, *Indian. J. Sci. Technol.* **4**, 666–669 (2011)
 - M.K. Kumar, S. Sudhahar, G. Bhagavannarayana, R. Mohan Kumar, Crystal growth, spectral, structural and optical studies of π -conjugated stilbazolium crystal: 4-Bromobenzaldehyde-4'-N'-methylstilbazolium tosylate. *Spectrochim. Acta Part A. Mol. Biomol. Spectros.* **125**, 79–89 (2014)
 - N.S. Sowmya, S. Sampathkrishnan, Y. Vidyakshmi, S. Sudhahar, R. Mohan Kumar, Synthesis, growth, structural, thermal and optical studies of pyrrolidinium-2-carboxylate-4-nitrophenol single crystals. *Spectrochim. Acta Part A Mol. Biomol. Spectros.* **145**, 333–339 (2015)
 - L.T. Cheng, W. Tam, S.R. Marder, A.E. Stiegman, G. Rikken, C.W. Spangler, Experimental investigations of organic molecular nonlinear optical polarizabilities. 2. A study of conjugation dependences. *J. Phys. Chem.* **95**, 10643–10652 (1991)
 - H.S. Nalwa, Organic materials for third-order nonlinear optics. *Adv. Mater.* **5**, 341–358 (1993)
 - M. Krishnakumar, S. Karthick, K. Thirupugalmani, S. Brahadeeswaran, Second and third-order nonlinear optical and DFT calculations on 2-amino-5-chloro pyridinium-L-tartrate: a phasematchable organic single crystal. *Opt. Mater.* **66**, 79–93 (2017)
 - A.A. Prasad, K. Muthu, M. Rajasekar, V. Meenatchi, S.P. Meenakshisundaram, Crystal growth, characterization and theoretical studies of 4-aminopyridinium picrate, *Spectrochim. Acta Part A: Mol. Biomol. Spectrosc.* **135**, 805–813 (2015)
 - V. Murugesan, M. Saravanabhavan, M. Sekar, Synthesis, characterization and pharmacological investigation of a new charge-transfer complex of 3-aminopyridinium- *p*-toluenesulfonate. *J. Mol. Struct.* **1084**, 95–102 (2015)
 - V. Murugesan, M. Saravanabhavan, M. Sekar, Synthesis, spectroscopic characterization and structural investigation of a new charge transfer complex of 2, 6-diaminopyridine with 4-nitrophenylacetic acid: antimicrobial, DNA binding/cleavage and antioxidant studies, *Spectrochim. Acta Part A: Mol. Biomol. Spectros.* **147**, 99–106 (2015)
 - B. Babu, J. Chandrasekaran, R. Thirumurugan, V. Jayaramakrishnan, K. Anitha, Experimental and theoretical investigation on 2-amino 5-bromopyridinium L-tartrate-A new organic charge-transfer crystal for optoelectronics device applications. *J. Mater. Sci. Mater. Electron.* **28**, 1124–1135 (2017)
 - L. Mariappan, A. Kandasamy, M. Rathnakumari, P. Sureshkumar, Synthesis, growth and properties of an organic nonlinear optical crystal: 2-aminopyridinium benzoate (2-APB). *J. Optik* **124**, 2630–2634 (2013)
 - N. Sundaraganesan, B.D. Joshua, T. Radjakoumar, Molecular structure and vibrational spectra of 2-chlorobenzoic acid by density functional theory and ab-initio Hartree-Fock calculations. *Indian J. Pure Appl. Phys.* **47**, 248–258 (2009)
 - A.S.L. Lee, Y.S. Li, Surface-enhanced Raman, normal Raman and infrared spectra of chlorobenzoic acids. *Spectrochim. Acta A Mol. Biomol. Spectrosc.* **52**, 173–184 (1996)
 - T.P. Srinivasan, S. Anandhi, R. Gopalakrishnan, Growth and characterization of 2-amino-4-picolinium 4-aminobenzoate single crystals. *Spectrochim. Acta Part A* **75**, 1223–1227 (2010)
 - R. Kaliammal, G. Parvathy, R. Mohan Kumar, M. Krishna Kumar, G. Vinitha, S. Sudhahar, Physicochemical and quantum chemical calculations on new bis (2-amino-6-methylpyridinium 3, 4-dimethoxybenzoate) dihydrate organic single crystal for third order nonlinear optical applications. *Chin. J. Phys.* **72**, 100–125 (2021)
 - L. Chandra, J. Chandrasekaran, K. Perumal, B. Babu, Third order nonlinear optical and electrical properties of new 2-aminopyridinium 2-chloro 4-nitrobenzoate single crystals. *Optik* **127**(6), 3206–3210 (2016)
 - B. Babu, J. Chandrasekaran, R. Thirumurugan, K. Anitha, M. Saravanabhavan, 2-Amino-6-methylpyridinium 4-nitrobenzoate: a phase matchable organic single crystal for optoelectronics device applications. *J. Mater. Sci.: Mater. Electron.* **28**, 9704–9716 (2017)
 - M. Krishnakumar, S. Karthick, K. Thirupugalmani, S. Brahadeeswaran, Second and third-order nonlinear optical and DFT calculations on 2-amino-5-chloro pyridinium-L-tartrate: A phasematchable organic single crystal. *Opt. Mater.* **66**, 79–93 (2017)
 - S.P. Jose, S. Mohan, Vibrational spectra and normal coordinate analysis of 2-aminopyridine and 2-amino picoline. *J. Spectrochim. Acta* **64**, 240–245 (2006)
 - N. Sundaraganesan, B. Dominic Joshua, T. Radjakoumar, Molecular structure and vibrational spectra of 2-chlorobenzoic acid by density functional theory and ab-initio Hartree-Fock calculations (2009)
 - P. Karuppasamy, T. Kamalesh, K. Anitha, S. Abdul Kalam, M. Senthil Pandian, P. Ramasamy, S. Verma, S. Venugopal Rao, Synthesis, crystal growth, structure and characterization of a novel third order nonlinear optical organic single crystal: 2-amino 4, 6-dimethyl pyrimidine-4-nitrophenol. *Opt. mater.* **84**, 475–489 (2018)
 - S.S. Solanki, N.P. Rajesh, T. Suthan, Growth and characterization of benzyl 4-hydroxybenzoate single crystal by vertical Bridgman technique for optical applications. *Opt. Laser Technol.* **103**, 163–169 (2018)

32. M. Magesh, G. Bhagavannarayana, P. Ramasamy, Synthesis, crystal growth and characterization of an organic material: 2-Aminopyridinium succinate succinic acid single crystal. *Spectrochim. Acta. Part A: Mol. Biomol. Spectros.* **150**, 765–771 (2015)
33. S. Venda, G. Peramaiyan, M. NizamMohideen, G. Vinitha, S. Srinivasan, Synthesis, growth, structural, thermal, dielectric, linear and nonlinear optical studies of 2-amino 6-methylpyridinium salicylate single crystal. *J. Optics* **46**, 149–157 (2017)
34. C.W. Tang, S.A. Vanslyke, Organic electroluminescent diodes. *Appl. Phys. Lett.* **51**, 913–915 (1987)
35. N. Siraj, F. Hasan, S. Das, L.W. Kiruri, K.E.S. Gall, G.A. Baker, I.M. Warner, Carbazole-derived group of uniform materials based on organic salts: solid state fluorescent analogues of ionic liquids for potential applications in organic-based blue light-emitting diodes. *J. Phys. Chem. C.* **118**, 2312–2320 (2014)
36. S. Sudhahar, M. Krishna Kumar, P. Pandi, R. Mohan Kumar, 2-Phenylethylammonium *p*-hydroxybenzoate, growth, structural, spectral, thermal, optical and mechanical characterization. *Optik* **125**(16), 4327–4332 (2014)
37. T. Suthan, N.P. Rajesh, C.K. Mahadevan, G. Bhagavannarayana, Studies on crystal growth and physical properties of 2-amino-5-chloropyridine single crystal *Mater. Chem. Phys.* **129**, 433–438 (2011)
38. S.L. Kakani, A. Kakani, *Mater. Sci.* (New Age International Publishers: New Delhi, 2004)
39. K. Sangwal, On the reverse indentation size effect and microhardness measurement of solids. *Mater. Chem. Phys.* **63**, 145–152 (2000)
40. E. Meyer, Untersuchungen über Härteprüfung und Härte Brinell Methoden, *Z. ver. Dtsch Ing.* **52** 645–654, (1908)
41. E.M. Onitsch, Über die mikrohart der metalle. *Microscopia* **2**, 131–151 (1947)
42. G. Parvathy, R. Kaliammal, K. Velsankar, M. Krishna Kumar, K. Sankaranarayanan, S. Sudhahar, Studies on structural, optical, homo-lumo and mechanical properties of piperazinium *p*-hydroxybenzoate monohydrate single crystal for nonlinear optical applications. *Chem. Phys. Lett.* **758**, 137934 (2020)
43. W.A. Wooster, properties and atomic arrangements in crystals. *Rep. Prog. Phys.* **16**, 62–82 (1953)
44. G. Pabitha, R. Dhanasekaran, Investigation on the crystal growth and characterization of an organometallic non linear optical crystal: Tetrathiourea mercury tetrathiocyanato manganate. *Mater. Sci. Eng. B* **177**, 1149–1155 (2012)
45. I. Fleming, *John wiley and Sons* (Frontier orbitals and organic chemical reactions, New York, 1976), p. 5
46. R.G. Pearson, electro negativity and hardness correlated with molecular orbital theory. *Proc. Natl. Acad. Sci.* **83**, 8440–8441 (1986)
47. R. Kaliammal, S. Sudhahar, G. Parvathy, K. Velsankar, K. Sankaranarayanan, Physicochemical and DFT studies on new organic Bis- (2-amino-6-methylpyridinium) succinate monohydrate good quality single crystal for nonlinear optical applications. *J. Mol. Struct.* **1212**, 128069 (2020)
48. M. Sheik-Bahae, A.A. Said, T. Wei, T.H. Hagand, D.J. Hagan, E.W. Van Stryland, *IEEE, J. Quant. Electron.* **26**, 760–779 (1990)
49. G. Vinitha, A. Ramalingam, Third-order optical nonlinearities and optical-limiting properties of a pararosanolin dye in liquid and solid media. *J. Laser Phys.* **18**, 1070–1073 (2008)
50. G. Jesby, M. George, J. Alex, D. Sajan, N.K. Shihab, G. Vinitha, R. Chitra, Growth of Morpholin-4-ium hydrogen tartrate single crystal for optical limiting application. *Opt. Laser Technol.* **119**, 105647 (2019)
51. V. Kannan, S. Brahadeeswaran, Synthesis, growth, thermal, optical and mechanical studies on 2-amino-6-methylpyridinium 4-hydroxybenzoate. *J. Therm. Anal. Calorim.* **124**, 889–898 (2016)
52. B. Punithaveni, K. Thilagavathy, N. Muthukumarasamy, D. Nithyaparakash, M. Saravanabhavan, Structural, spectral, electrical, Z-scan and HOMO LUMO studies on new 2-amino-6-methylpyridinium 2-hydroxybenzoate crystal. *Mater. Sci. Pol.* **36**, 537–546 (2018)
53. M. Krishnakumar, S. Karthick, K. Thirupugalmani, B. Babu, G. Vinitha, Growth, spectral, optical, laser damage threshold and DFT investigations on 2-amino 4-methyl pyridinium 4-methoxy benzoate (2A4MP4MB): a potential organic third order nonlinear optical material for optoelectronic applications. *Opt. Laser Technol.* **101**, 91–106 (2018)
54. J.H. Joshi, S. Kalainathan, M.J. Joshi, K.D. Parikh, Influence of l-serine on microstructural, spectroscopic, electrical and nonlinear optical performance of ammonium dihydrogen phosphate single crystal. *J. Mater. Sci. Mater. Electron.* **30**, 14243–14255 (2019)
55. J.H. Joshi, K.P. Dixit, K.D. Parikh, H.O. Jethva, D.K. Kanchan, S. Kalainathan, M.J. Joshi, Effect of Sr²⁺ on growth and properties of ammonium dihydrogen phosphate single crystal. *J. Mater. Sci. Mater. Electron.* **29**, 5837–5852 (2018)

Publisher's Note Springer Nature remains neutral with regard to jurisdictional claims in published maps and institutional affiliations.